Journal of Magnetism and Magnetic Materials 374 (2015) 663–668

Contents lists available at ScienceDirect

Journal of Magnetism and Magnetic Materials

journal homepage: www.elsevier.com/locate/jmmm

Study of magnetoelastic and magnetocrystalline anisotropies in Co_xNi_{1-x} nanowire arrays

Anastasiia Moskaltsova [a,b,*], Mariana P. Proenca [c], Sergey V. Nedukh [d], Célia T. Sousa [c], Arthur Vakula [d], Gleb N. Kakazei [c,e], Sergey I. Tarapov [d], Joao P. Araujo [c]

[a] National Technical University Kharkiv Polytechnic Institute, 21, Frunze Str., 61002 Kharkiv, Ukraine
[b] INESC-MN, Rua Alves Redol, 9-1, 1000-029 Lisbon, Portugal
[c] IFIMUP and IN Institute of Nanoscience and Nanotechnology and Dep. Física e Astronomia, Univ. Porto, Rua do Campo Alegre 687, 4169-007 Porto, Portugal
[d] O. Ya. Usikov Institute for Radiophysics and Electronics of the National Academy of Sciences of Ukraine, 12, Proskura str., 61085 Kharkov, Ukraine
[e] Institute of Magnetism National Academy of Sciences of Ukraine, 36b Vernadskogo Blvd., 03142 Kiev, Ukraine

ARTICLE INFO

Article history:
Received 5 June 2014
Received in revised form
5 August 2014
Available online 19 September 2014

Keywords:
Anodic aluminum oxide template
Co–Ni alloy
DC electrodeposition
Ferromagnetic resonance
Nanowire

ABSTRACT

Highly ordered Co_xNi_{1-x} nanowire (NW) arrays were electrodeposited inside nanoporous anodic aluminum oxide membranes. The control of the applied potential during the electrodeposition process allowed us to easily tune the Co% in the alloy. Systematic studies on the morphological and crystallographic properties together with static and dynamic magnetic characterizations were performed. In this work we focus on the study of the dynamic magnetic properties of CoNi NW arrays using the ferromagnetic resonance method at both room (RT) and low (LT) temperatures. The careful comparison analysis performed between the magnetic anisotropy fields obtained at RT and LT, allowed us to extract for the first time the magnetocrystalline anisotropy effect of the Co component and, most importantly, the magnetoelastic anisotropy effect of Ni.

1. Introduction

Nanoporous anodic aluminum oxide (AAO) membranes have attracted significant attention in recent years, as excellent templates for the low-cost fabrication of ordered arrays of nanowires (NWs) and nanotubes [1–3]. The combination of these templates with simple filling methods allows one to easily tune the final geometrical parameters of the grown nanostructures, such as diameter, interwire distance, length, composition and tube wall thickness [4,5]. Among the several materials deposited inside AAO templates, magnetic NWs stand out, as they are of great interest in modern technology and science [6,7]. Due to their large surface areas and high aspect ratios, magnetic NW arrays have become promising materials for the novel magnetic storage devices [8,9], and already had been used to improve existing ones [10]. In particular, CoNi alloy has proved to be a very interesting magnetic material, as it can exhibit either a soft or a hard magnetic behavior, depending on the Co content in the alloy [11–14]. This can be easily controlled by the deposition conditions thus achieving a wide range of Co:Ni ratios, which will then allow one to better tune the magnetic response of these systems.

The magnetic properties of the novel two-dimensional magnetic nanostructures are of significant interest in both fundamental and applied research. High frequency studies are favored in NWs as their diameters are smaller than the skin depth [15,16]. One of the most powerful techniques to characterize such nanostructures is the ferromagnetic resonance (FMR) method that gives information on the magnetization, magnetic anisotropy, dipolar interactions, relaxation of magnetization dynamics as well as on the structural quality and (in)homogeneity [17,18] of the nanomagnet arrays. FMR is the most suitable technique for determining the abovementioned magnetic properties of single NWs and their arrays [15,19,20], and will thus be used here to characterize CoNi NW arrays.

In this work, highly ordered CoNi NW arrays with different Co content were successfully fabricated inside the AAO nanoporous membranes. Systematic measurements of the morphology, composition and structure, together with the magnetic studies, were performed. The structural properties are found to correlate well with the static and dynamic magnetic results and show a strong dependence of the magnetic properties on the Co% in the studied NW arrays. The effective anisotropy field of the fabricated NW arrays was extracted from experimental FMR results. The combination of both RT and LT FMR measurements, allowed us to

* Corresponding author at: INESC-MN, Rua Alves Redol, 9-1, 1000-029 Lisbon, Portugal.
E-mail address: amoskaltsova@inesc-mn.pt (A. Moskaltsova).

http://dx.doi.org/10.1016/j.jmmm.2014.09.036
0304-8853/

simultaneously extract the magnetocrystalline anisotropy (mostly caused by Co) and the magnetoelastic anisotropy (mostly caused by Ni) in the fabricated NW arrays.

2. Experimental details

Ordered hexagonal arrays of Co_xNi_{1-x} NWs with diameters of ~50 nm, interwire distances of ~115 nm, aspect ratios (AR; length/diameter) between 273 and 420 and different Co contents ($0.64 < x < 0.90$), were successfully grown by a potentiostatic electrodeposition technique inside nanoporous AAO templates. The AAO membranes were fabricated by a two-step anodization process of high-purity (>99.997%) aluminum foils [1], in 0.3 M oxalic acid at 40 V and 5 °C. The first and second anodization processes were performed for 24 and 48 h, respectively, in order to obtain AAO membranes with ordered hexagonal arrays of pores and membrane thicknesses of ~70 μm. Additional details on the membranes preparation can be found elsewhere [21–23]. For the further potentiostatic electrodeposition process inside the AAO nanopores, the Al substrate was removed by chemical etching in a 0.2 M $CuCl_2$ and 4.1 M HCl aqueous solution at room temperature. The alumina barrier layer present at the bottom of the pores was then etched by ion milling, and a 100 nm thick Ag film was sputtered on the back side of the pores to serve as the working electrode during the deposition process. The electrodeposition of the CoNi NW arrays was performed at 35 °C using a Watts-type bath with 64.5% of Co^{2+} ions (0.71 M $CoSO_4$, 0.09 M $CoCl_2$, 0.38 M $NiSO_4$, 0.06 M $NiCl_2$, and 0.73 M H_3BO_3) [11]. During the electrodeposition process a Pt mesh served as a counter electrode and Ag/AgCl (in 4 M KCl) as the reference electrode. The tuning of the Co content was achieved by varying the deposition potential in the range of −1.1 V to −1.5 V vs. Ag/AgCl. The morphological properties and chemical composition of the fabricated CoNi NW arrays were studied using scanning electron microscopy (SEM; FEI Quanta 400 FEG) and energy dispersive X-ray spectroscopy (EDS), respectively. Structural analysis was performed by means of X-ray diffraction (XRD; PANalytical X'Pert Pro) using Cu $K_{\alpha 1}$ radiation ($\lambda = 0.15406$ nm) and the Bragg–Brentano $\theta/2\theta$ geometry. The static magnetic characterization of the NW arrays was performed at room temperature using a superconducting quantum interference device (SQUID) magnetometer from Quantum Design. The magnetic dynamical properties of the fabricated NW arrays were systematically studied using the FMR method at both low (LT) and room (RT) temperatures [24,25]. The dynamic magnetic characterization was carried out at Radiospectroscopy Dept. IRE NAS of Ukraine. The LT measurements were performed at 4.2 K (liquid helium) in the frequency range 70–78 GHz. The RT experiments were carried out in the K (18–26.5 GHz) and Ka (26.5–40 GHz) frequency bands.

3. Results and discussion

3.1. Morphological and compositional characterization

CoNi NW arrays were successfully fabricated by the DC electrodeposition method. The morphological studies of the produced NWs were performed using SEM imaging. Prior to bottom SEM imaging the contact layer was removed by ion beam milling (200 nm). Fig. 1 shows SEM images of both bottom [Fig. 1(a) and (b)] and cross-sectional [Fig. 1(c)] views, illustrating the high order of the hexagonal array and the uniform length distributions obtained with this technique. The NWs diameters d and lengths L were estimated by SEM, and are summarized in Table 1. Interwire distance D_{int} is found to be constant for all the samples as well as pore filling percentages P, $D_{int} = 115 \pm 5$ nm and $P = 95\%$ respectively. To determine the compositional ratio of Co and Ni in the NW arrays, energy dispersive X-ray spectroscopy (EDS) has been used. The obtained spectra allowed us to quantify the Co% of the NW arrays (Table 1) and determine its dependence on the electrodeposition potential E [11,22,26].

3.2. Crystallographic structure

XRD studies showed the presence of mixed crystallographic structures of face-centered cubic (*fcc*) Ni and Co, textured along the [220] direction, and hexagonal closed packed (*hcp*) Co, textured along the [100] direction, depending on the Co% content (Fig. 2). For the NWs with higher Co content we can observe a mixture of *fcc* and *hcp* crystallographic structures, but with *hcp* dominating. In the case of less Co content we have the inverse situation: there is also a mixture of phases but now with an increased *fcc* structure. Such behavior has already been reported by Vivas et al. [12] and Vega et al. [11,26] and was expected in the investigated arrays, as the increase in Ni content was previously shown to facilitate the growth of the *fcc* structure.

3.3. Magnetization hysteresis measurements

Magnetic hysteresis $M(H)$ loops were measured for all the samples at RT in both parallel (∥) and perpendicular (⊥) directions of the applied magnetic field (H) to the NW long axis [Fig. 3(a)–(c)]. The $M(H)$ loops behavior is found to depend significantly on the Co% content of the measured NW arrays. Fig. 3(d) summarizes the variation of coercivity (H_c) and reduced remanence ($m_r = M_r/M_s$, where M_r is the remanence and M_s is the saturation magnetization) with the Co% content of the studied NW arrays. The coercivity obtained for parallel magnetic field measurements is always bigger than the one for the field applied perpendicular ($H_c^{\parallel} > H_c^{\perp}$), regardless of the Co content of the alloy, which indicates the shape anisotropy domination. In addition, both coercivity and

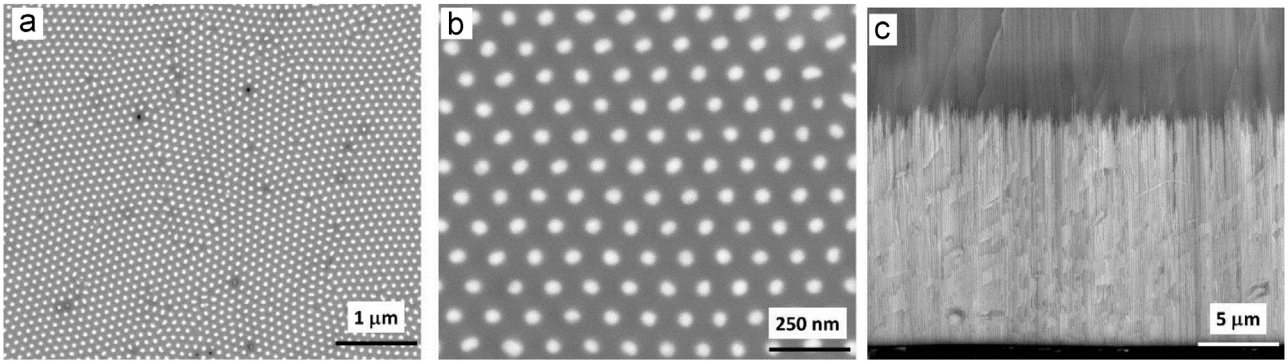

Fig. 1. SEM images of the fabricated CoNi NW arrays: (a) and (b) bottom, and (c) cross-sectional views. Note the different scales.

remanence, measured along the NW long axis, are found to increase with Co% [Fig. 3(d)], due to the Co hardening effect, which reinforces the magnetic anisotropy. Thus, for the Co-rich NW array ($Co_{0.9}Ni_{0.1}$), where one would expect the magnetocrystalline anisotropy to set the favorable direction perpendicular to the NW long axis [Figs. 2(c) and 3(c)], we still have domination of the shape anisotropy, favoring an easy axis of magnetization parallel to the NW axis. However, when increasing the Ni% content of the NW arrays, the coercivity values for both parallel and perpendicular measurements become relatively close ($H_c^{\parallel} \approx H_c^{\perp}$), and the remanence along the perpendicular direction increases [Fig. 3(d)], becoming higher than the remanence along the parallel direction ($m_r^{\perp} > m_r^{\parallel}$). This evidences a change of the easy magnetization axis to the perpendicular direction for the sample $Co_{0.64}Ni_{0.36}$, which indicates that by adding Ni to the sample we transform it into a soft sample [27], and most likely form multidomains in the Co–Ni system [13]. The obtained dependencies are different from the ones recently reported by Vivas et al. [12] for CoNi NW arrays with small diameters (35 nm). Nevertheless, the results presented in this paper are in accordance with the ones reported by Pereira et al. [27] for CoNi NWs with 50 nm in diameter, where the authors have obtained higher coercivity values when increasing the Co% content. In addition, Pereira et al. have also found differences in the magnetic behavior of their samples when compared to the results previously obtained by Vivas et al. [12]. However, the magnetic behavior obtained in this work and in reference [27] are both similar to the one measured in larger diameter nanowires (130 nm), where the coercivity tends to decrease as the percentage of Ni in the alloy increases [11]. Talapatra et al. [13] have also obtained different trends for the magnetic behavior of CoNi alloy nanowires with tuned compositions, electrodeposited in alumina templates with pore diameters of ~250 nm. The authors suggest that the CoNi system is composed

Table 1
Main parameters of the fabricated NW arrays: diameter (d), length (L) and aspect ratio (AR).

Sample	Co%	Electrodeposition potential E, V	d (nm)	L (μm)	AR
S1	90	−1.1	44 ±2	12 ±0.5	273
S2	78	−1.3	50 ±2	21 ±0.5	420
S3	64	−1.5	51 ±2	14 ±0.5	275

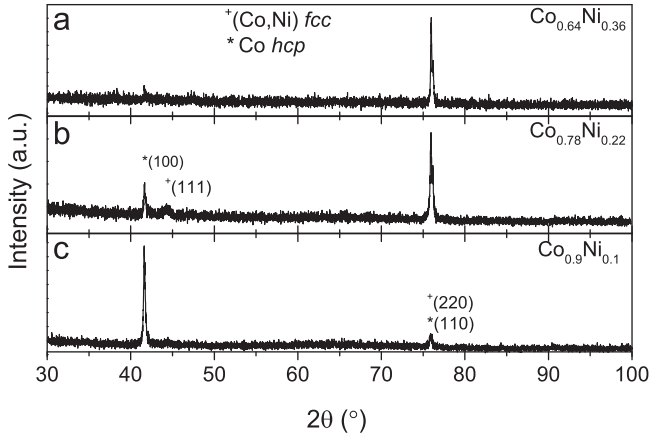

Fig. 2. Experimental XRD spectra of the fabricated CoNi NW arrays.

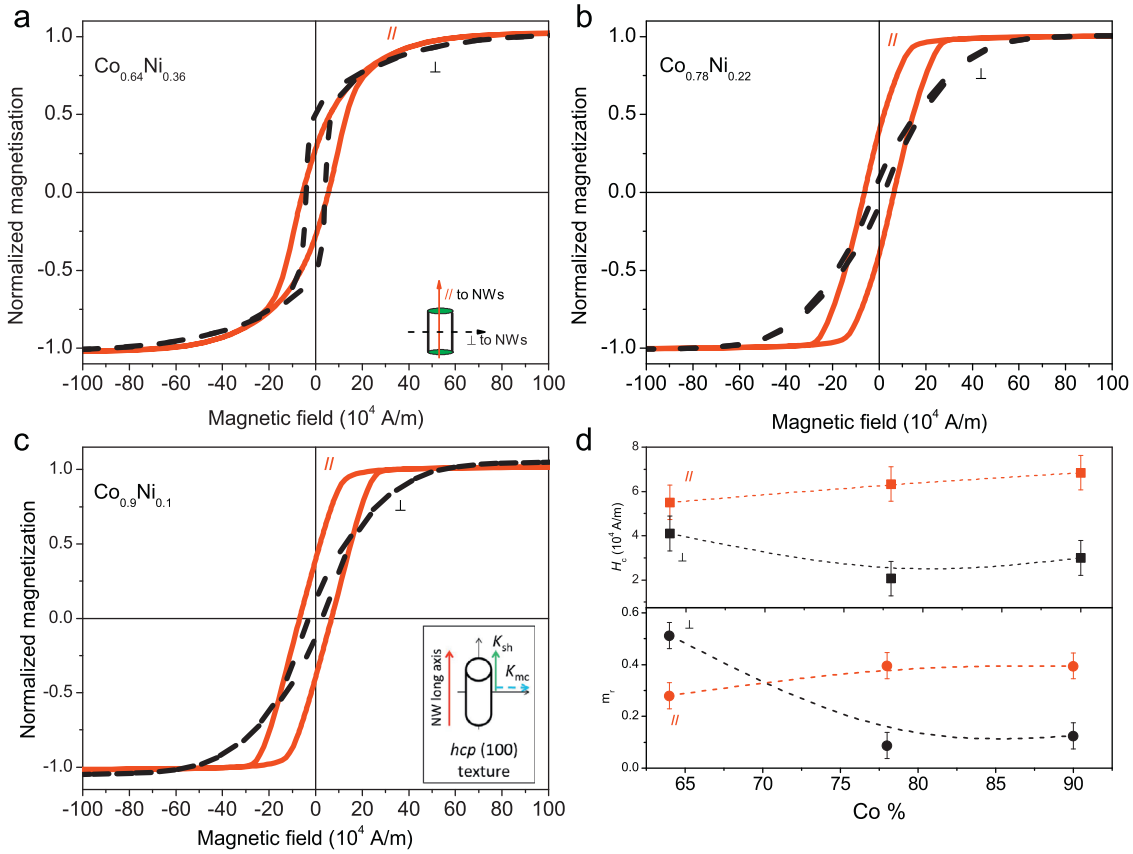

Fig. 3. (a)–(c) Magnetic hysteresis loops of the fabricated CoNi NW arrays, measured with the magnetic field applied parallel (∥, red solid line) and perpendicular (⊥, black dashed line) to the NW long axis. The inset in (c) is a schematic representation of the shape (K_{sh}) and magnetocrystalline (K_{mc}) anisotropy directions of a Co NW textured along the *hcp* [100] direction. (d) Dependence of the reduced remanence (m_r) and the coercivity (H_c) of the CoNi NW arrays on the Co% content. Lines are guides for eye. (For interpretation of the references to color in this figure caption, the reader is referred to the web version of this article.)

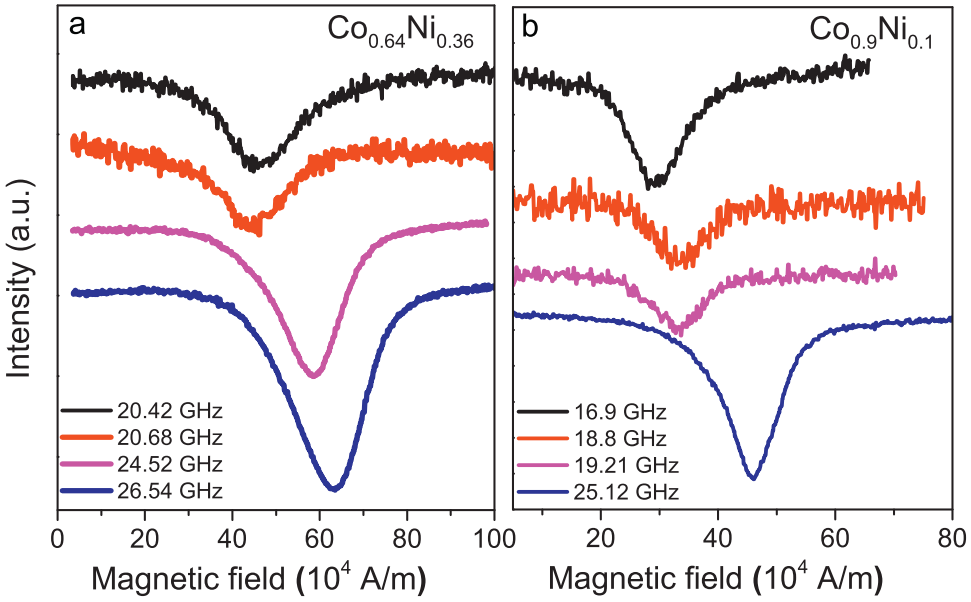

Fig. 4. Experimental FMR absorption spectra measured at room temperature for (a) $Co_{0.64}Ni_{0.36}$ and (b) $Co_{0.9}Ni_{0.1}$ NWs.

of multidomains when the cobalt concentration is lower than 55%, which then leads to coercivity degradation.

3.4. Ferromagnetic resonance measurements

To better understand the magnetic contributions to the effective anisotropy field of the fabricated CoNi NW arrays, FMR studies were performed at both RT and LT on the samples with the lowest ($Co_{0.64}Ni_{0.36}$) and highest ($Co_{0.9}Ni_{0.1}$) Co% content with magnetic field applied along NWs long axis. Fig. 4 shows the experimental absorption peaks obtained for the two studied samples at RT. One can observe that the increase of Co% content leads to a decrease of the resonance magnetic field (H_{res}). Additionally, the signal to noise (SNR) ratio is also seen to improve with the frequency increase.

Fig. 5 summarizes the results obtained at room temperature, showing the dependencies of the resonance frequencies (f_{res}) on the resonance fields (H_{res}) for the two studied samples, $Co_{0.9}Ni_{0.1}$ and $Co_{0.64}Ni_{0.36}$. Analyzing the obtained results we extracted the effective anisotropy field (H_{eff}^{exp}) values by interpolation of the experimental frequency-field dependencies with the equation [2,13]:

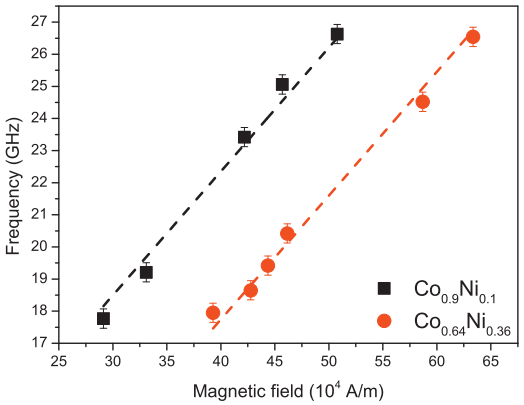

Fig. 5. Frequency-field dependencies of the $Co_{0.9}Ni_{0.1}$ and $Co_{0.64}Ni_{0.36}$ NW arrays, measured at RT.

$$f_{res} = \gamma(H_{res} - H_{eff}^{exp}) \quad (1)$$

where γ is the gyromagnetic ratio which is assumed to be 3.07 MHz/Oe for our samples [19,28]. The obtained values of the H_{eff}^{exp} are presented in Table 2.

To further study the magnetic anisotropies that exist in CoNi NW arrays, we have calculated the theoretical resonance fields (H_{eff}^{calc}) of the NW arrays and compared those with the experimentally obtained values (H_{eff}^{exp}). From the magnetic hysteresis loops measured at RT (Fig. 3) we have already seen that the magnetic effective anisotropy field is dominated by shape anisotropy. The shape anisotropy field (H_{sh}) of NW arrays can be estimated as $H_{sh} = 2\pi(3f - 1)M_s$ [18,29], where M_s is the saturation magnetization and f is the volumetric filling factor that depends on the arrays geometry and is defined as $f = \pi d^2/(2\sqrt{3}D_{int}^2)$. However, one should note that this is only correct for perfectly filled pores (P=100%). If the pore filling fraction is lower, this should be taken into account when estimating the value of H_{sh}. Therefore, in this work we have determined H_{sh} as $H_{sh} = 2\pi(3fP - 1)M_s$, where $f \sim 0.15$ is the volumetric filling factor, P=95% is the pore filling factor measured by SEM, and M_s is the saturation magnetization of the CoNi NWs, that was calculated using the Slater–Pauling curve [30]. H_{eff}^{calc} can then be defined as [31]

$$H_{eff}^{calc} = H_{sh} - H_{\perp} \quad (2)$$

where $H_{\perp}$ represents a perpendicular anisotropy field, corresponding to the additional anisotropy contributions presented in the fabricated NWs [26,32]. By comparing the experimental and calculated values of H_{eff} ($H_{eff}^{exp} = H_{eff}^{calc}$) we were able to estimate the values of $H_{\perp}$ for CoNi NWs with different Co% content (Table 2). In addition, since at RT one can neglect the effect of the magnetoelastic anisotropy field (H_{me}) arising from the Ni content, we are thus able to estimate the magnetocrystalline anisotropy field (H_{mc}) by assuming $H_{\perp} = H_{mc}^{RT}$. Despite the fact that the electrolyte solution used during the electrodeposition process was heated up to 35 °C, the temperature difference in this case will not cause significant magnetoelastic effect as it was reported previously [33]. Moreover, the magnetocrystalline anisotropy of Ni is considerably lower than the one of Co ($K_{mc}^{Ni} = -4 \times 10^4$ J/m^3 vs. $K_{mc}^{Co(hcp)} = 4.1 \times 10^5$ J/m^3) [32,33], so we can state that $H_{\perp}^{RT} = H_{mc}^{Co(RT)}$, and thus estimate the

Table 2
Experimental and calculated values of the magnetic anisotropy fields of CoNi NW arrays with different Co% content.

Sample	Co%	M_s (emu/cm^3)	H_{sh}, 10^4 A/m	H_{eff}^{exp}, 10^4 A/m (RT)	H_{eff}^{exp}, 10^4 A/m (LT)	$H_{mc}^{RT} = H_{mc}^{LT}$, 10^4 A/m	$H_{\perp}^{LT}$, 10^4 A/m	H_{me}, 10^4 A/m
S1	90	1329	−41 ±1	−18 ±1	−8 ±1	−23 ±2	−33 ±2	−10 ±2
S3	64	1101	−27 ±1	−6 ±1	10 ±1	−21 ±2	−37 ±2	−16 ±2

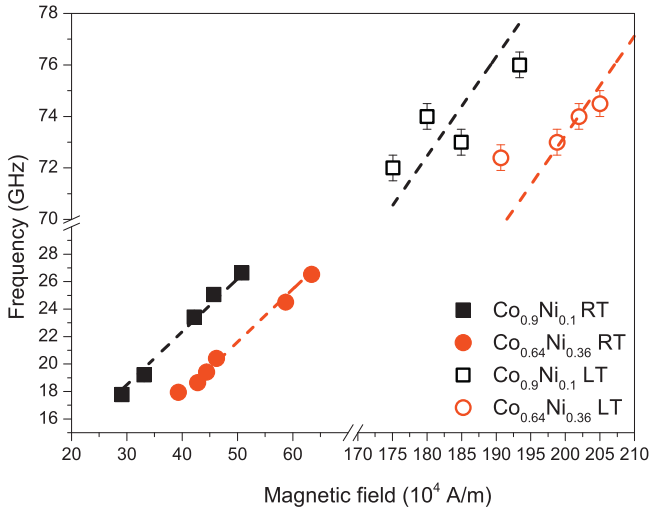

Fig. 6. Frequency-field dependencies of the $Co_{0.9}Ni_{0.1}$ and $Co_{0.64}Ni_{0.36}$ NW samples, measured at both room (RT) and low (LT) temperatures.

magnetocrystalline anisotropy field of Co in both samples. Table 2 summarizes the results obtained for samples $Co_{0.9}Ni_{0.1}$ and $Co_{0.64}Ni_{0.36}$, where an increase of $|H_{mc}|$ with Co% content is observed, as expected [12]. In order to study the magnetoelastic effect of the Ni component (that is expected to increase with temperature decrease [33,34]) in the fabricated NW arrays, low-temperature FMR measurements were performed. Fig. 6 shows the frequency-field dependencies of the RT and LT FMR measurements performed for samples $Co_{0.9}Ni_{0.1}$ and $Co_{0.64}Ni_{0.36}$. Using Eq. (1) to interpolate the LT results plotted in Fig. 6, and assuming H_{sh} is independent of temperature, we extracted the values of $H_{\perp}^{LT}$, which are summarized in Table 2. This additional anisotropy field comes mainly from the magnetocrystalline anisotropy field of Co and the magnetoelastic anisotropy field of Ni, and thus one expects $H_{\perp}^{LT} \approx H_{mc}^{Co} + H_{me}^{Ni}$. In addition, since the magnetocrystalline anisotropy constant of Co does not change much with temperature [35], we can assume $H_{mc}^{Co(LT)} \approx H_{mc}^{Co(RT)}$, which was already extracted from the RT FMR measurements. Therefore, combining RT and LT FMR results we were able to estimate the magnetoelastic effect of Ni in CoNi NW arrays. The values obtained are summarized in Table 2. As expected, $|H_{me}|$ is found to increase with the Ni% content in the CoNi samples. This additional effect of magnetoelastic anisotropy component arising at LT comes from the magnetoelastic coupling between magnetostriction and mechanical stress caused by the large mismatch between the thermal expansion coefficients of AAO and Ni [32,33,36]. Recent studies by Tannous et al. [37] show temperature dependence of the effective magnetic field in Ni NW arrays, while in this work we only performed FMR experiments at two extreme temperatures: 4.2 K and 300 K. Therefore, further studies should be performed in order to better understand the nature of the anisotropies behavior.

In summary, the effective magnetic anisotropy field of CoNi NWs comprises several different components: a strong shape anisotropy field due to the high aspect-ratio of the NWs; a magnetocrystalline anisotropy field arising from the Co content; and a magnetoelastic anisotropy field due to the presence of Ni. The careful comparative analysis of RT and LT FMR measurements allowed us to estimate the values of the different anisotropies present in CoNi NWs with tuned Co%. The change of the effective anisotropy field at RT and LT occurs due to the interplay between magnetocrystalline and magnetoelastic anisotropies.

4. Conclusions

CoNi NW arrays were successfully fabricated by electrodeposition growth inside nanoporous AAO templates. XRD structural studies illustrated the presence of a mixture of *fcc* and *hcp* crystallographic Co structures. Their ratio was tuned by the Co content, which gave us a higher *hcp* texture in the Co rich sample. The dependence of the coercivity and remanence magnetization on the Co content of the studied NW arrays was obtained from magnetization hysteresis loops. Using FMR results, measured at both RT and LT, we determined the effective anisotropy field of the samples. The obtained values were used to extract the magnetocrystalline and magnetoelastic contributions and it was concluded that with increasing Co% we have higher magnetocrystalline anisotropy constant, and with increasing Ni% we enhance the magnetoelastic anisotropy field. Summarizing, the accurate control of the Co:Ni ratio determines the respective magnetic properties of the NW arrays, in particular the magnetic anisotropy fields, which are very important for their future implementation in next generation devices and systems.

Acknowledgments

AM acknowledges financial support from the Ministry of Education and Science, Youth and Sports of Ukraine, ord. No 755 dated 27.06.2012. MPP, CTS and GNK are thankful to FCT for grants SFRH/BPD/84948/2012, SFRH/BPD/82010/2011 and IF/00981/2013, respectively. The authors acknowledge funding from FEDER and ON2 through project Norte-070124-FEDER-000070 and from FCT under projects FEDER/POCTI/n2-155/94, PTDC/CTM/NAN/115125/2009 and through the Associated Laboratory – IN.

References

[1] H. Masuda, K. Fukuda, Ordered metal nanohole arrays made by a two-step replication of honeycomb structures of anodic alumina, Science 268 (1995) 1466.
[2] N. Nielsch, F. Muller, A.P. Li, U. Gosele, K. Fukuda, Uniform nickel deposition into ordered alumina pores by pulsed electrodeposition, Adv. Mater. 12 (8) (2000) 582–586.
[3] R. Inguanta, M. Butera, C. Sunseri, S. Piazza, Fabrication of metal nanostructures using anodic alumina membranes grown in phosphoric acid solution: tailoring template morphology, Appl. Surf. Sci. 253 (2007) 5447–5456.
[4] M.P. Proenca, C.T. Sousa, J. Ventura, M. Vazquez, J.P. Araujo, Distinguishing nanowire and nanotube formation by the deposition current transients, Nanoscale Res. Lett. 7 (2012) 280.
[5] X.-F. Han, S. Shamaia, R. Sharif, J.-Y. Chen, H.-R. Liu, D.-P. Liu, Structural and magnetic properties of various ferromagnetic nanotubes, Adv. Mater. 21 (2009) 1–6.

[6] L. Zhang, T. Petit, K.E. Peyer, B.J. Nelson, Targeted cargo delivery using a rotating nickel nanowire, Nanomed. Nanotech. Biol. Med. 8 (7) (2012) 1074–1080.
[7] L. Savage, Artificial photosynthesis: saving solar energy for a rainy day, Opt. Photonics News 24 (2) (2013) 18–25.
[8] G. Hrkac, J. Dean, D.A. Allwood, Nanowire spintronics for storage class memories and logic, Phil. Trans. R. Soc. A. 369 (2011) 3214–3228.
[9] X. Kou, X. Fan, R.K. Dumas, Q. Lu, Y. Zhang, H. Zhu, X. Zhang, K. Liu, J.Q. Xiao, Memory effect in magnetic nanowire arrays, Adv. Mater. 23 (11) (2011) 1393–1397.
[10] S.S.P. Parkin, M. Hayashi, L. Thomas, Magnetic domain-wall racetrack memory, Science 320 (2008) 190–194.
[11] V. Vega, T. Bohnert, S. Martens, M. Waleczek, J.M. Montero-Moreno, D. Gorlitz, V.M. Prida, K. Nielsch, Tuning the magnetic anisotropy of Co–Ni nanowires: comparison between single nanowires and nanowire arrays in hard-anodic aluminum oxide membranes, Nanotechnology 23 (2012) 465709.
[12] L.G. Vivas, M. Vazquez, J. Escrig, S. Allende, D. Altbir, D.C. Leitao, J.P. Araujo, Magnetic anisotropy in CoNi nanowire arrays: analytical calculations and experiments, Phys. Rev. B 85 (2012) 035439.
[13] S. Talapatra, X. Tang, M. Padi, T. Kim, R. Vajtai, G.V.S. Sastry, M. Shima, S. C. Deevi, P.M. Ajayan, Synthesis and characterization of cobalt nickel alloy nanowires, J. Mater. Sci. 44 (9) (2009) 2271–2275.
[14] S.L. Cheng, C.N. Huang, Template synthesis of large-scale single-crystalline Co–Ni alloy nanowire arrays by electrochemical deposition, Syn. React. Inorg. Met. 38 (2008) 475.
[15] M. Demand, A. Encinas-Oropesa, S. Kenane, U. Ebels, I. Huynen, L. Piraux, Ferromagnetic resonance studies of nickel and permalloy nanowire arrays, J. Magn. Magn. Mater. 249 (2002) 228–233.
[16] R. Arias, D.L. Mills, Theory of spin excitations and the microwave response of cylindrical ferromagnetic nanowires, Phys. Rev. B 63 (2001) 134439.
[17] G.N. Kakazei, Y.G. Pogorelov, M.D. Costa, T. Mewes, P.E. Wiegen, P.C. Hammel, V.O. Golub, T. Okuno, V. Novosad, Origin of fourfold anisotropy in square lattices of circular ferromagnetic dots, Phys. Rev. B 74 (2006) 060406.
[18] G. Kakazei, P.E. Wigen, K.Y. Guslienko, R.W. Chantrell, N.A. Lesnik, V. Metlushko, H. Shima, K. Fukamichi, Y. Otani, V. Novosad, In-plane and out-of-plane uniaxial anisotropies in rectangular arrays of circular dots studied by ferromagnetic resonance, J. Appl. Phys. 93 (10) (2003) 8418.
[19] C.A. Ramos, E. Vasallo Brigneti, M. Vázquez, Self-organized nanowires: evidence of dipolar interactions from ferromagnetic resonance measurements, Phys. B 354 (2004) 195.
[20] U. Ebels, J.-L. Duvail, P.E. Wigen, Ferromagnetic resonance studies of Ni nanowire arrays, Phys. Rev. B 64 (2001) 144421.
[21] D.C. Leitao, A. Apolinario, C.T. Sousa, J. Ventura, J.B. Sousa, M. Vazquez, J. P. Araujo, Nanoscale topography: a tool to enhance pore order and pore size distribution in anodic aluminum oxide, J. Phys. Chem. C 115 (17) (2011) 8567–8572.
[22] A. Moskaltsova, M.P. Proenca, C.T. Sousa, A. Apolinario, J. Ventura, G.N. Kakazei, J.P. Araujo, Influence of the electrodeposition cathodic potential on the composition and magnetic properties of CoNi nanowire, Solid State Phenom. 214 (2014) 32–39.
[23] M.P. Proenca, C.T. Sousa, J. Ventura, M. Vazquez, J.P. Araujo, Ni growth inside ordered arrays of alumina nanopores: enhancing the deposition rates, Electrochim. Acta 72 (2012) 215–221.
[24] S.I. Tarapov, Y.P. Machekhin, A.S. Zamkovoy, Magnetic Resonance for Optoelectronic Materials Investigating, Collegium, Kharkov, 2008.
[25] F. Yildiz, B.Z. Rameev, S.I. Tarapov, L.R. Tagirov, B. Aktas, High-frequency magnetoresonance absorption in amorphous magnetic microwires, J. Magn. Magn. Mater. 247 (2002) 222–229.
[26] J. Garcia, V. Vega, L. Iglesias, V.M. Prida, B. Hernando, E.D. Barriga-Castro, R. Mendoza-Resendez, C. Luna, D. Gorlitz, K. Nielsch, Template assisted Co–Ni alloys and multisegmented nanowires with tuned magnetic anisotropy, Phys. Status Solidi A 211 (2014) 1041–1047.
[27] A. Pereira, C. Gallardo, A.P. Espejo, J. Briones, L.G. Vivas, M. Vazquez, J. C. Denardin, J. Escrig, Tailoring the magnetic properties of ordered 50-nm-diameter CoNi nanowire arrays, J. Nanopart. Res. 15 (2013) 2041.
[28] M. Darques, A. Encinas, L. Vila, L. Piraux, Controlled changes in the microstructure and magnetic anisotropy in arrays of electrodeposited co nanowires induced by the solution pH, J. Phys. D: Appl. Phys. 37 (2004) 1411.
[29] C.T. Sousa, D.C. Leitão, M.P. Proença, A. Apolinário, A.M. Azevedo, N.A. Sobolev, S.A. Bunyaev, Y.G. Pogorelov, J. Ventura, J.P. Araújo, G.N. Kakazei, Probing the quality of Ni filled nanoporous alumina templates by magnetic techniques, J. Nanosci. Nanotechnol. 12 (2012) 7486–7490.
[30] S. Chikazumi, Physics of Ferromagnetism, 2nd ed., Oxford University Press, Oxford, UK, 1997.
[31] G.N. Kakazei, A.F. Kravets, N.A. Lesnik, M.M. Pereira de Azevedo, Y. G. Pogorelov, J.B. Sousa, Ferromagnetic resonance in granular thin films, J. Appl. Phys. 85 (1999) 5654.
[32] L.G. Vivas, M. Vazquez, V. Vega, J. Garcia, W.O. Rosa, R.P. del Real, V.M. Prida, Temperature dependant magnetization in Co-base nanowire arrays: role of crystalline anisotropy, J. Appl. Phys. 111 (2012) 07A325.
[33] D.C. Leitao, J. Ventura, C.T. Sousa, A.M. Pereira, J.B. Sousa, M. Vazquez, J. P. Araujo, Insights into the role of magnetoelastic anisotropy in the magnetization reorientation of magnetic nanowires, Phys. Rev. B 84 (2011) 014410.
[34] A. Kumar, S. Fahler, H. Schlorb, K. Leistner, L. Schultz, Competition between shape anisotropy and magnetoelastic anisotropy in Ni nanowires electrodeposited within alumina templates, Phys. Rev. B 73 (2006) 064421.
[35] R.M. Bozorth, Ferromagnetism, Wiley, USA, 1993.
[36] K.R. Pirota, E.L. Silva, D. Zanchet, D. Navas, M. Vazquez, M. Hernandez-Velez, M. Knobel, Size effect and surface tension measurements in Ni and Co nanowires, Phys. Rev. B 76 (2007) 233410.
[37] C. Tannous, A. Ghaddar, J. Gieraltowski, Temperature dependent anisotropy and elastic effects in ferromagnetic nanowire arrays, arXiv:1104.5348v3 [cond-mat.mtrl-sci].